ACS OMEGA

Open Access

http://pubs.acs.org/journal/acsodf

Article

"3E" Analysis and Working Fluid Selection for a Cogeneration System for Geothermal Large Temperature Difference Utilization

Jiahui Yin, Bing Zhu,* Yiming Zhang, and Jinsen Huang

Cite This: *ACS Omega* 2024, 9, 16221−16236

Read Online

ACCESS | Metrics & More | Article Recommendations

ABSTRACT: Widespread utilization of geothermal energy as a clean energy source can reduce the use of fossil fuels and thereby protect the environment. Previous combined heat and power (CHP) systems using low-temperature geothermal heat as a heat source have limited utilization of geothermal heat. In this study, a cogeneration system based on organic Rankine cycle (ORC) and absorption heat exchanger (AHE) is designed. We analyzed the thermal efficiency, exergy efficiency, and economics of the proposed system utilizing 85 °C low-temperature geothermal heat, and the optimal operating fluid for this system is discussed. The results show that the optimal working fluid for the proposed system is R245fa. Using R245fa as the working fluid, the proposed system can achieve an exergy efficiency of 61.39%, when the heat source outlet temperature can be as low as 23 °C, while the proposed system can achieve the lowest LCOE of 0.082 ($/kW ·h) when using R22 as the working fluid.

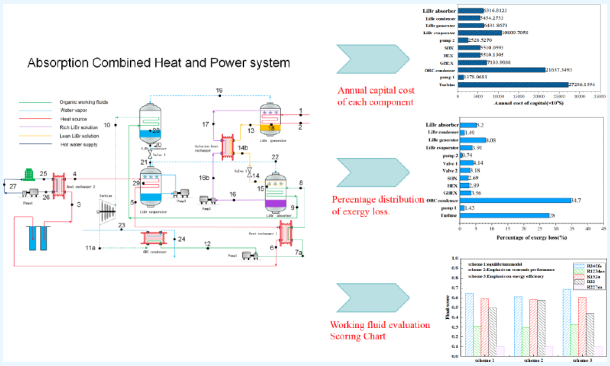

1. INTRODUCTION

In the present era, the burning of fossil fuels has led to a significant climate crisis, which is a shared global challenge confronting the international community at present.[1] To address this issue, governments have implemented various initiatives and policies aimed at identifying eco-friendly energy alternatives to fossil fuels.[2] The utilization of green energy sources can successfully mitigate carbon emissions and contribute to achieving the goals of 'peak carbon' and 'carbon neutrality' established by individual nations.[3] Among the myriad green energy sources available, geothermal energy stands out as a clean and sustainable energy option with minimal environmental impact.[4] Geothermal energy is abundant and boasts a substantial reservoir, estimated at approximately 3.6 × 1014 GWh within the Earth.[5] Furthermore, the carbon emission factor associated with geothermal power generation is considerably lower than that of thermal power generation, positioning geothermal power as a pivotal player in the journey toward carbon neutrality. Due to these aforementioned advantages, geothermal energy, as a renewable energy source, has garnered high esteem from countries across the globe.[6]

As of now, geothermal heat can be harnessed for power generation or direct thermal applications, contingent on the geothermal resource's temperature and the complexity of extraction. Geothermal resources categorized as dry-thermal-rock types, with temperatures exceeding 200 °C, are often employed as heat sources for the dry steam power cycle. In this method, dry steam is extracted from geothermal wells, purified through filtration to remove larger solid particles, and then channeled into a steam turbine to produce electricity.[7] This approach is well-established and cost-effective. On the other hand, more widely available geothermal resources are typically hydrothermal geothermal resources with lower to medium temperatures, typically below 150 °C. These resources are better suited for the flash steam power cycle and binary power cycle.[8] It is important to note that geothermal power plants relying solely on low to medium temperature geothermal resources may encounter substantial drilling costs. Consequently, they might struggle to compete economically with conventional power plants unless they receive corresponding feed-in tariff subsidies. In response to this challenge, low-temperature geothermal energy, with temperatures below 90 °C, can be directly utilized for various purposes, including residential heating, bathing, greenhouse operations, irrigation, and agricultural production, employing a cogeneration approach.[9] This cogeneration system enables the gradual use of the heat source, enhancing energy efficiency and spreading operational expenses.[10,11] It offers a practical solution to the economic challenges associated with low-temperature geo-

Received: December 21, 2023
Revised: March 10, 2024
Accepted: March 13, 2024
Published: March 26, 2024

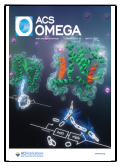

thermal resources.[12] Therefore, with the aim of improving the overall efficiency of thermal resource utilization and the economic viability of low-temperature geothermal resources, the focus has shifted toward the multigeneration use of low-temperature geothermal resources.

When it comes to combined heat and power generation using low-temperature geothermal sources, the organic Rankine cycle (ORC) stands out as the most commonly employed power generation cycle.[13] ORC systems offer a range of advantages, including a compact design, high stability, ease of installation and maintenance, and strong economic efficiency.[14] Furthermore, ORC is well-suited for converting low-temperature heat into electricity, making it a prevalent choice in waste heat recovery and thermoelectric conversion systems.[15] However, optimizing the ORC system to effectively match the temperature of the heat source presents a notable challenge, as temperature differences between pinch points ('pinch points' refer to abrupt or critical points of temperature variation along the heat flow path) can result in substantial thermal energy losses. Previous research efforts have concentrated on various aspects of optimization to enhance the ORC systems for geothermal applications. These areas of focus include the selection of appropriate working fluids,[16] optimization of key operational parameters,[17] refinement of system components,[18] exploration of advanced system architectures,[19] and the pursuit of cogeneration strategies.[20] In the literature, a combination of experimental and numerical studies has investigated these optimization measures. The key findings from these efforts are summarized as follows:

Javanshir et al.[21] developed a comprehensive methodology for the selection of the most suitable working fluid in ORC systems with a reheaters (regenerative ORC), taking into account both cycle conditions and the thermophysical properties of the working fluid. Their findings revealed that the incorporation of a return heater in the ORC cycle could mitigate variations in the thermal efficiency among different working fluids without affecting the net output ratio. They conducted a series of comparisons on the thermodynamic performance of 14 different working fluids in subcritical, superheated, and transcritical states. Their conclusion pointed to R113 having the best performance in the system, as it exhibited the highest specific net output. In a separate study, Hu et al.[22] developed an organic Rankine cycle system specifically engineered for generating power from low-temperature geothermal sources. They examined the thermodynamic characteristics of five organic working fluids with the primary assessment criterion being the net power generation per unit mass of geothermal water. Their research revealed that five organic working fluids with similar thermal properties were suitable for the system, and among these, R245fa was identified as the most appropriate working fluid. In another investigation, Zhao et al.[23] further refined the system's performance parameters based on the choice of the working fluid. They optimized an ORC system for low enthalpy geothermal brine by employing five distinct working fluids. Under conditions with brine inlet temperatures of 120 and 100 °C, they identified the optimal working fluids for the system as R1224yd(Z) and R1336mzz(Z), respectively, with the goal of maximizing the net circulating power of the system. Their results underscore the need to select the appropriate working materials for operation of the system under varying working conditions.

Furthermore, the advanced cogeneration configurations for geothermal organic Rankine cycle (ORC) systems have garnered significant interest in recent research. Guzovic et al.[24] utilized 175 °C geothermal heat to generate electricity using a dual-pressure ORC (there are two different pressure levels in the working cycle.). Their system comprises both high- and low-pressure circuits, with initial mass separation occurring at the start of evaporation within the high-pressure circuit. The minimum mass flow required for preheating in the high-pressure circuit is directed to the high-pressure preheater, while the remaining mass is channeled to the low-pressure circuit. The data indicate that the hot water cooling curve in the dual-pressure ORC closely aligns with the mass heating/boiling curve. This approach not only reduces thermodynamic losses in the geothermal water-work fluid heat exchanger during heat transfer but also optimizes the ORC system components. Consequently, the dual-pressure ORC demonstrates enhanced efficiency and net power compared to the standard ORC, with efficiency increasing from 52% to 65% and net power rising from 5,270 kW to 6,371 kW. In a separate study, Eyerer et al.[25] have developed an advanced ORC−CHP architecture using a 135 °C geothermal heat source. This design involves extracting partially expanded vapor from an expander and directing it to a low-pressure preheater for work fluid regeneration and preheating. This approach improves heat source utilization and enables the system to adapt flexibly to fluctuations in the load of the district heating system (DHS), achieving a minimum load of 15.3%. However, in recent years, more advanced thermocoupled configurations in series or parallel have been proposed. To comprehensively compare these CHP architectures, Erdeweghe et al.[26] conducted simultaneous investigations into series, parallel, preheated parallel, and HB4 structures (HB4 structures: a hybrid of series and parallel) for CHP. The results consistently demonstrate that, when connected to a 65/40 DH system with geothermal temperatures ranging from 110 to 150 °C, the efficiency of various cogeneration modes consistently exceeds that of a pure power plant. Among the structures studied, the HB4 configuration outperforms the others, displaying the highest power output (HB4 > preheated parallel > series > parallel). Notably, the HB4 structure achieves an efficiency of 56.8%, representing a 22.8% improvement compared to that of a pure power plant. Furthermore, based on the ORC dichotomy, Ma et al.[27] developed a CCHP system utilizing geothermal resources. This innovative system comprises an absorption refrigeration cycle, a heat exchange cycle, and an organic Rankine cycle. The total thermal efficiency of the system was 41.17% and 84.93% during the cooling and heating seasons, respectively, with exergy efficiency figures of 47.28% and 62.23%. However, it is important to note that the system described in this literature may not operate efficiently when dealing with low-temperature geothermal sources below 90 °C. This limitation arises due to temperature differences between the pinch points, and the ORC system may not adequately address the issue of high heat source outlet temperatures, which often exceed 40 °C.[28,29]

The concept of the absorption heat exchanger (AHE), as introduced by Sun et al.[30] presents a promising solution to the previously mentioned issue. The AHE combines the functionality of a heat exchanger and an absorption heat pump. This combination enables the harnessing of waste heat for effective heat exchange, resulting in a final outlet temperature on the cold side that is lower than the initial

https://doi.org/10.1021/acsomega.3c10250
ACS Omega 2024, 9, 16221−16236

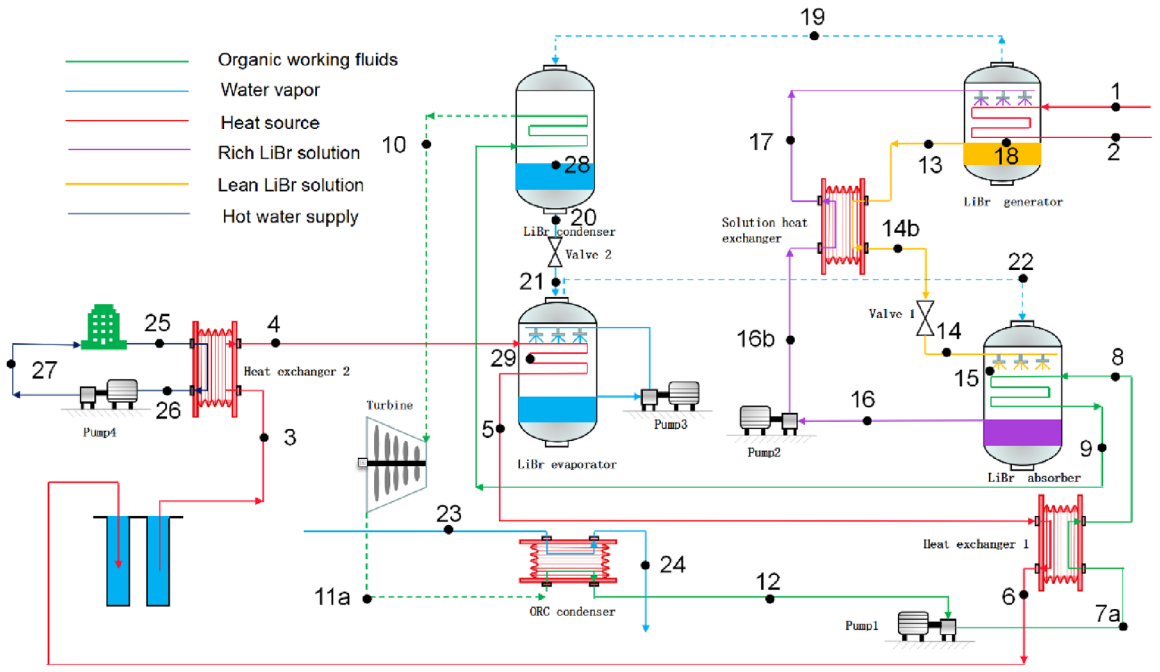

Figure 1. Schematic diagram of the ACHP.

inlet temperature. This innovation realizes heat exchangers with large temperature differentials, thereby improving the overall efficiency. Integrating the AHE into the ORC system effectively addresses the pinch point temperature concern within the ORC. Building upon this concept, Xie et al.[31] developed an AHE system capable of recovering heat sources with temperatures ranging from 65 to 70 °C. This represents a substantial increase in the temperature difference delivered, doubling what is achievable with conventional heat exchangers.

It is noteworthy that many researchers have primarily focused on the direction of absorption heat pumps (AHPs). As an illustration, Zhang et al.[32] introduced a combined cogeneration system that integrates organic Rankine cycle and absorption heat pump technologies for the recovery of condensing waste heat from a power plant's turbine. The implementation of this system resulted in a 4.01% increase in overall efficiency and a 11.97% boost in capacity for the power plant. Dogbe et al.[33] constructed a waste heat recovery system using AHP and ORC to assess cogeneration performance in a sugar plant. The AHP system saved 0.83% of the heat energy from sugar cane combustion, leading to a 1.7% improvement in energy efficiency. Khalilzadeh et al.[34] suggested an innovative system integrating AHP and CCHP. This combined approach led to a 17.68% enhancement in energy efficiency compared to the original CCHP system when operating with a low-temperature heat source at 90 °C. Additionally, the system reduced the investment cost of the CCHP system configuration by 32.65% by using biomass as the heat source. However, it is essential to note that the studies mentioned above primarily focused on enhancing overall energy utilization. There was no increase in energy efficiency for the ORC system, and the problem of high temperatures at the heat source out of the system was not addressed. In contrast, Tian et al.[35] made a significant breakthrough by designing a two-stage absorption heat exchanger (AHE) and integrating it into an ORC system, resulting in a high-efficiency cogeneration system known as AHEORC−CHP (The absorption heat exchanger coupled ORC combined heat and power system.) This innovative AORC system effectively harnessed waste heat sources, reducing the heat source temperature to 24.69 °C while achieving a high-temperature efficiency of 1.2 and a thermoelectric efficiency of 90.9%. It is important to note that while both AHP and AHE coupled with ORC systems have been applied in industrial waste heat research, there is currently no geothermal cogeneration ORC system with an integrated AHE system.

In light of the existing literature, this paper proposes an innovative system referred to as absorption combined heat and power (ACHP), which is based on an absorption heat exchanger (AHE) in combination with an ORC system. The ACHP system proposed in this paper uses an AHE as the evaporator in the ORC system. This integration capitalizes on the AHE's ability to facilitate heat exchange with a large temperature difference and combines it with the power generation capacity of the ORC. This allows the low-temperature heat source to be exchanged multiple times in the shell heat exchanger within the AHE system. This characteristic significantly reduces the heat source outlet temperature and enhances the utilization of geothermal energy for both power generation and heat production. The system outlined in this paper is crafted for the integration of 85 °C low-temperature geothermal resources into a unified district heating and power generation system. It efficiently utilizes geothermal water in a gradual manner and effectively addresses the challenge of high geothermal return water temperatures. To enhance the thermodynamic and economic analysis of the ACHP system, this paper explores critical parameters including the geothermal mass flow rate, the outlet temperature of the geothermal in AHE, the temperature of the heat source exiting the AHE evaporator, and the evaporation temperature of the organic working fluid. Energy, exergy, and economic analysis methods are proposed to analyze the system performance. These parameters are examined for five potential working fluids. In the realm of research methodologies, when

https://doi.org/10.1021/acsomega.3c10250
ACS Omega 2024, 9, 16221−16236

confronted with multiple performance objectives, the optimization of system design inevitably involves methods such as multiobjective optimization and multiobjective decision-making. Wang et al.[36] employed multiobjective optimization techniques to optimize the thermodynamic performance and overall cost per unit of product in a CCHP system, resulting in the attainment of comprehensive performance limits. Additionally, in another ORC system, Wang et al.[37] utilized multiobjective decision-making approaches to analyze factors including thermodynamics, economics, and the environment. This approach, compared to multiobjective optimization, offers a more comprehensive assessment of working fluid performance. Furthermore, the paper introduces an integrated evaluation method, denoted as FAHP-EWM (fuzzy analytic hierarchy process-entropy weight method), which leverages these parameters to determine the optimal working fluids. The selection is based on a combination of criteria, such as the levelized cost of electricity (LCOE), exergy efficiency, and thermal efficiency.

2. SYSTEM DESCRIPTION

Figure 1 depicts the working principle of the ACHP (absorption combined heat and power) model. This system shares fundamental principles with the ORC system, with the distinction that the absorption heat exchanger substitutes for the evaporator. And a heat exchanger for district heating is added. The absorption heat exchanger (AHE) integrates both an absorption heat pump (AHP) and a heat exchanger (HEX). The AHP comprises five primary components: an evaporator, an absorber, a condenser, a generator, and a solution heat exchanger. The ACHP comprises three cycles: the solution cycle, the process cycle, and the district heating cycle. In the AHP, water serves as the working medium for the solution cycle, while lithium bromide acts as the absorbent in the process cycle. Proper selection of the working fluid and solution can lead to higher energy conversion efficiency and lower capital costs. Water is an ideal recycling working fluid; lithium bromide has a high boiling point, good solubility in water, and excellent stability, making it suitable for use as an absorbent.[38] Only requiring a minimal driving heat source temperature, the characteristics of the H_2O/LiBr solution combination's boiling point differential enable the recovery of low-temperature heat. H_2O/LiBr is more efficient compared to the NH_3/H_2O solution commonly used in refrigeration systems. As a result, LiBr and H_2O are selected as the work fluid and solution for AHP, respectively. The district heating cycle refers to the user end side, where the water in the heat exchanger is exchanged with geothermal heat.

The function of the AHE in the ACHP model is the same as that of the evaporator in the ORC system, and a 150 °C medium-temperature heat source enters the generator at point 1 to serve as the driving heat source. The 85 °C low-temperature geothermal heat source is directed to the heat exchanger, where it undergoes heat exchange with the heating water for the user-side. Subsequently, it passes through the evaporator in the AHE before entering the HEX for further heat exchange and ultimately returning underground. For the organic working fluid in the ORC, after pump 1, it enters the HEX for preheating and then subsequently proceeds through the absorber and condenser within the AHE system to create superheated steam. Superheated steam expands through the turbine for expansion and power generation, and eventually, the working fluid is cooled as it passes through the condenser, transitioning into a liquid state to enter the subsequent cycle. The ACHP system allows the low-temperature geothermal heat to supply heat to area residents before exchanging heat with AHE's low-pressure evaporator. This arrangement allows the heat source to be utilized in multiple steps in multiple components, giving the AHE's evaporator a higher evaporation temperature. Increasing the temperature of the initial ORC working fluid during turbine operation results in a higher efficiency. This effect is observed when the concentration difference in the solution combination remains constant. This arrangement makes full use of the energy of the heat source, reduces the temperature of the heat source at the exit of the system, and improves the overall energy efficiency, as well as the energy efficiency of the ORC system.

3. MODELING AND ANALYSIS

The ACHP system uses the following assumptions in the modeling and calculation process:[35,39] (1) The system operates in a state of thermal equilibrium and stability, without considering heat exchange with the surroundings. (2) The working fluid achieves saturation at the outlets of the evaporator and condenser, reaching thermal equilibrium. (3) The system's kinetic and potential energy can be regarded as negligible. (4) The working fluid at the absorber and generator outlets is a saturated solution, and there is no under-absorption or under-absorption occurring. (5) With the exception of pumps and valves, the pressure loss between components is negligible. (6) The work of the solution and solvent pumps are neglected.

The constant parameters required for the calculation are given in Table 1.

Table 1. Constant Parameters Assumed for ACHP Performance Evaluation

parameter	value	reference
driving heat source temperature (K)	423.15	/
geothermal source temperature (K)	358.15	/
specific heat at constant pressure for the hot gas ($kJ\cdot kg^{-1}\cdot K^{-1}$)	1.1	40
environment temperature (K)	298.15	41
environment pressure (kPa)	101.3	41
condensing temperature (K)	303.15	42
pump isentropic efficiency	0.7	40
cooling water temperature (K)	293.15	43
minimum temperature difference of heat exchangers (K)	10.0	42

3.1. Energy Analysis. Based on eqs 1−3, the points of the system are established on mass balance, material balance, and energy balance, and the equations can be found in Table 2. Furthermore, eq 4 provides the expression for the electrical efficiency of the system. Furthermore, eq 4 provides the expression for the electrical efficiency[44] of the system.

$$\sum \dot{m} = 0 \tag{1}$$

$$\sum \dot{m}x = 0 \tag{2}$$

$$\sum \dot{Q} + \dot{W} + \dot{m}h = 0 \tag{3}$$

$$\eta_{elc} = \frac{\dot{W}_{net}}{\dot{Q}_{tot}} \tag{4}$$

https://doi.org/10.1021/acsomega.3c10250
ACS Omega 2024, 9, 16221−16236

Table 2. Equations Governing the Mass, Material, and Energy Balances of the Systems

component	equation
LiBr evaporator	$\dot{m}_{21} = \dot{m}_{22}$
	$\dot{Q}_{eva,AHE}=\dot{m}_{22}h_{22} - \dot{m}_{21}h_{21}$
LiBr generator	$\dot{m}_{17} = \dot{m}_{19} + \dot{m}_{13}$
	$\dot{m}_{13\times13} = \dot{m}_{17\times17}$
	$\dot{Q}_{gen,AHE} = \dot{m}_{13}h_{13} + \dot{m}_{19}h_{19} - \dot{m}_{17}h_{17}$
LiBr absorber	$\dot{m}_{16} = \dot{m}_{22} + \dot{m}_{14}$
	$\dot{m}_{14\times14} = \dot{m}_{16\times16}$
	$\dot{Q}_{abs,AHE} = \dot{m}_{22}h_{22} + \dot{m}_{14}h_{14} - \dot{m}_{16}h_{16}$
LiBr condenser	$\dot{m}_{19} = \dot{m}_{20}$
	$\dot{Q}_{con,AHE} = \dot{m}_{19}h_{19} - \dot{m}_{20}h_{20}$
solution heat exchanger	$\dot{m}_{13} = \dot{m}_{14b}\ \dot{m}_{16b} = \dot{m}_{17}$
	$\dot{Q}_{SHE} = \dot{m}_{13}h_{13} - \dot{m}_{14}\ h_{14b} = \dot{m}_{17}h_{17} - \dot{m}_{16}h_{16b}$
heat exchanger 1	$\dot{m}_{7a} = \dot{m}_{8}$
	$\dot{Q}_{HEX} = \dot{m}_{5}h_{5} - \dot{m}_{6}h_{6} = \dot{m}_{8}h_{8} - \dot{m}_{7a}h_{7a}$
heat exchanger 2	$\dot{m}_{4} = \dot{m}_{3}\ \dot{m}_{25} = \dot{m}_{26}$
	$\dot{Q}_{HEX} = \dot{m}_{3}h_{3} - \dot{m}_{4}h_{4} = \dot{m}_{26}h_{26} - \dot{m}_{25}h_{25}$
ORC evaporator	$\dot{m}_{7a} = \dot{m}_{10}$
	$\dot{Q}_{eva,ORC} = \dot{m}_{10}h_{10} - \dot{m}_{7a}h_{7a}$
ORC condenser	$\dot{m}_{23} = \dot{m}_{24}$
	$\dot{Q}_{con,ORC} = \dot{m}_{23}h_{23} - \dot{m}_{24}h_{24}$
turbine	$\dot{m}_{11a} = \dot{m}_{10} = \dot{m}_{11}$
	$\dot{W}_{tur,ORC} = \dot{m}_{11a}h_{11a} - \dot{m}_{10}h_{10} = (\dot{m}_{11}h_{11} - \dot{m}_{10}h_{10})\eta_{tur}$
pump 1	$\dot{m}_{7a} = \dot{m}_{7} = \dot{m}_{12}$
	$\dot{W}_{pump1} = \dot{m}_{7a}h_{7a} - \dot{m}_{12}h_{12} = (\dot{m}_{7}h_{7} - \dot{m}_{12}h_{12})\eta_{pump1}$
pump 2	$\dot{m}_{21} = \dot{m}_{22}$
	$\dot{W}_{pump2} = \dot{m}_{16b}h_{16b} - \dot{m}_{16}h_{16}$
valve 1	$\dot{m}_{14} = \dot{m}_{14b}$
	$\dot{m}_{14\times14} = \dot{m}_{14b\times14b}$
valve 2	$\dot{m}_{20} = \dot{m}_{21}$

In the equation, $\dot{W}_{net}$ represents the net power of the system on the generation side of the ORC, and $\dot{Q}_{tot}$ represents the total energy gained from the heat source and is calculated using the following equation:

$$\dot{W}_{net} = W_{tur} - W_{pump1} - W_{pump2} - W_{pump3} \tag{5}$$

$$\dot{Q}_{tot} = \dot{m}(h_1 - h_2 + h_4 - h_6) \tag{6}$$

where $\dot{m}$ represents the mass flow rate of the work fluid, which can be expressed as

$$\dot{m} = \frac{\dot{m}_{wh}C_{p,wh}(T_1 - T_2) + \dot{m}_{gw}C_{p,gw}(T_1 - T_2)}{h_{10} - h_{7a}} \tag{7}$$

where $\dot{m}_{wh}$ and $C_{p,wh}$ represent the mass flow rate and isobaric specific heat capacity of waste heat, while $\dot{m}_{gw}$ and $C_{p,gh}$ represent the mass flow rate and isobaric specific heat capacity of geothermal water, respectively.

The thermal efficiency of the system is defined as follows:

$$\eta_{elc} = \frac{\dot{W}_{net} - W_{pump4} + Q_{rh}}{\dot{Q}_{tot} + Q_{rh}} \tag{8}$$

which Q_{rh} represents the heat gained by residential buildings

$$Q_{rh} = \dot{m}(h_3 - h_4) \tag{9}$$

COP is used to express the result of energy analysis, which is usually defined in air conditioning as the ratio of accepted thermal energy to consumed electrical energy. And COP in heat pumps is defined in different ways by different scholars. In this paper, the definition of AHE[30] on the study of Sun et al. is selected: COP is determined by the ratio of the evaporator heat load to the generator heat load, providing a distinctive measure of AHE efficiency. This way of defining the COP is usually less than 1 in AHE studies.[30,45] Here, COP less than 1 is not a poor performance but a difference in the way it is defined. The expression for COP is as follows:

$$\mathrm{COP} = \frac{\dot{Q}_{eva,AHE}}{\dot{Q}_{gen,AHE}} \tag{10}$$

3.2. Exergy Model. Exergy is an effective energy that the system can theoretically convert into work. In this study, when kinetic energy and potential energy are neglected, it is composed of physical and chemical energy. Its expression is

$$\dot{E} = \dot{E}_{ph} + \dot{E}_{ch} \tag{11}$$

where $\dot{E}_{ph}$ is the physical exergy.

$$\dot{E}_{ph} = \dot{m}[(h_i - h_0) - T_0(S_i - S_0)] \tag{12}$$

The chemical exergy, denoted as $\dot{E}_{ch}$, originates from the aqueous lithium bromide solution in the ACHP system.

$$\dot{E}_{ch} = \sum \dot{Z}_i b_i \tag{13}$$

where $\dot{Z}_i$ and b_i represent the molar fraction of each component and the reference chemical energy, respectively. The chemical energy is shown in Table 3.

Table 3. Reference Chemical Exergy for Each Component[46a]

component	b_{H2O}	b_{Li}	b_{Br}
value (kJ/mol)	8.62	371.96	34.33

[a]Reprinted (Adapted or Reprinted in part) with permission from ref46. Copyright (2020) (Elsevier).

However, since there is no chemical process involved in the ORC system, the final exergy is expressed as follows:

$$\dot{E} = \dot{m}[(h_i - h_{0)} - T_0(S_i - S_0)] \tag{14}$$

The parameters h_i and S_i signify the enthalpy and entropy, respectively, under ambient temperature and pressure conditions.

The formula for calculating the system's efficiency is given by

$$\eta_{ex,sys} = \frac{\dot{E}_{all} - \sum \dot{I}}{\dot{E}_{all}} \tag{15}$$

The sum of energy losses in each component is denoted by $\sum \dot{I}$, and the exergy loss equations for each component of the system are outlined in Table 4.

Introducing a metric to visually quantify the system's efficiency in utilizing energy from the heat source, the concept of heat source energy utilization can be expressed in the following mathematical form:

$$\eta_{ex,sou} = \frac{\dot{E}_{all} - \sum \dot{I}}{\dot{E}_{sou}} \tag{16}$$

https://doi.org/10.1021/acsomega.3c10250
ACS Omega 2024, 9, 16221−16236

Table 4. Formulas for Conducting an Exergy Analysis of the System

component	equation
LiBr evaporator	$\dot{I}_{eva,AHE} = \dot{E}_{21} - \dot{E}_{22} + Q_{eva,AHE}\left(1 - \frac{T_0}{T_{eva,AHE}}\right)$
LiBr generator	$\dot{I}_{gen,AHE} = \dot{E}_{17} - \dot{E}_{13} - \dot{E}_{19} + Q_{eva,AHE}\left(1 - \frac{T_0}{T_{gen,AHE}}\right)$
LiBr absorber	$\dot{I}_{abs,AHE} = \dot{E}_{22} + \dot{E}_{14} - \dot{E}_{16} + Q_{abs,AHE}\left(1 - \frac{T_0}{T_{abs,AHE}}\right)$
LiBr condenser	$\dot{I}_{con,AHE} = \dot{E}_{19} - \dot{E}_{20} - Q_{con,AHE}\left(1 - \frac{T_0}{T_{con,AHE}}\right)$
solution heat exchanger	$\dot{I}_{SHE} = \dot{E}_{16b} + \dot{E}_{13} - \dot{E}_{17} - \dot{E}_{14b}$
heat exchanger 1	$\dot{I}_{HEX} = \dot{E}_{5} + \dot{E}_{7a} - \dot{E}_{8} - \dot{E}_{6}$
heat exchanger 2	$\dot{I}_{HEX} = \dot{E}_{3} + \dot{E}_{25} - \dot{E}_{4} - \dot{E}_{26}$
ORC evaporator	$\dot{I}_{eva,ORC} = \dot{E}_{1} + \dot{E}_{4} + \dot{E}_{7a} - \dot{E}_{2} - \dot{E}_{10}$
ORC condenser	$\dot{I}_{con,ORC} = \dot{E}_{23} + \dot{E}_{11a} - \dot{E}_{24} - \dot{E}_{12}$
turbine	$\dot{I}_{tur,ORC} = \dot{E}_{10} - \dot{E}_{11a} - \dot{W}_{tur}$
pump 1	$\dot{I}_{pum1} = \dot{E}_{12} - \dot{E}_{7a} + \dot{W}_{pum1}$
pump 2	$\dot{I}_{pum2} = \dot{E}_{16b} - \dot{E}_{16}$
valve 1	$\dot{I}_{val1} = \dot{E}_{14} - \dot{E}_{14b}$
valve 2	$\dot{I}_{val2} = \dot{E}_{21} - \dot{E}_{20}$

$\dot{E}_{sou}$ represents the total energy of the heat source prior to entering the system.

3.3. Economic Model. In the economic feasibility analysis, the total cost comprises both investment and operational costs, with the investment cost encompassing equipment expenses for all system components. Geothermal activation energy for the plant is derived from a standard geothermal well with low-temperature geothermal resources at a depth of 200m. The cost of geothermal wells is presented in eq 17, which can be adapted for geothermal wells with depths ranging from 200 m to 400 m. Reinjection wells are chosen from geothermal wells with a typical depth of 70 m, and their cost is defined in eq 18.[47,48]

$$C_{GW} = 2150\left[\frac{\$}{m}\right]L_{GW} \tag{17}$$

$$C_{RW} = 7556.4[\$] + 64.02\left[\frac{\$}{m}\right]L_{W} + 0.0058\left[\frac{\$}{m^2}\right]L_{W} \tag{18}$$

The driving heat source for the absorption heat exchanger in this system is provided by hot steam at 150 °C. Due to factors such as coal prices, regional disparities, and electricity rates, there is no standardized pricing for industrial steam across different regions. In this study, we employ a calorimetric valuation method to calculate the cost of steam. The relevant parameters for steam and the method of heat measurement are derived from the Chinese national standard (GB/T 34060-2017)[49] with the steam heat formula specified in eq 19. The heat charge is set at 12.65$/GJ, based on the charging standards for nonresidential metered heat established by the municipal government of Beijing, China.[50] The steam cost is given in eq 20

$$Q = \int_{t_2}^{t_1} q_m \triangle h'' \mathrm{d}t \tag{19}$$

$$C_{st} = 12.65[\$] \times \frac{Q}{10^{\times 6}} \tag{20}$$

Regarding the heat exchanger cost:

$$\log C_b = K_1 + K_2 \log A + K_3 (\log A)^2 \tag{21}$$

where K is the parameter, A is the heat exchange area, and C_b is the basic cost.

The cost of pumps and turbines:

$$\log C_b = K_1 + K_2 \log W + K_3 (\log W)^2 \tag{22}$$

where W is the turbine power.

C_b represents the fundamental cost of each component and is determined based on the assumption that the component operates at ambient pressure. However, these components often cannot operate under the standard conditions. Therefore, equipment costs must account for variables like temperature, pressure, and other nonstandard operating conditions. Consequently, it is essential to make cost adjustments by considering the impact of these factors.

Correction equation for plate heat exchangers:

$$C_e = C_b(B_1 + B_2 F_M F_P) \tag{23}$$

where C_e is the parameter-corrected cost and F_M and F_P are the material correction factor and pressure correction factor, respectively. The formula F_P is as follows:

$$\log F_P = Z_1 + Z_2 \log P + Z_3 (\log P)^2 \tag{24}$$

where P represents the operating pressure of the equipment.

Corrective equation of the turbine:

$$C_e = C_b F_{bm} \tag{25}$$

Where F_{bm} is the correction parameter. The correction factors for eqs 21−25 can be found in Table 5.

The correction parameter, F_{bm}, is introduced, and the correction factors for eqs 21−25 are specified in Table 5.

When calculating the cost of a heat exchanger, the total cost is primarily determined by its heat transfer surface area, which is

Table 5. Formulas for Conducting the Exergy Analysis of the System[51a]

component	K_1	K_2	K_3	B_1	B_2	C_1	C_2	C_3	F_M	F_{bm}
HX-P	4.6656	−0.1557	0.1547	0.96	1.21	0	0	0	1.0	/
HX-S	4.8306	−0.8509	0.3187	1.63	1.66	0	0	0	1.30	/
					(5 < p < 140 barg)	0.03881	−0.11272	0.08183		
turbine	2.2476	1.4965	−0.1618	/	/	/	/	/	/	3.30
pump	3.3892	0.0536	0.1538	1.89	1.35	0	0	0	1.50	/
					(10 < p < 100 barg)	−0.3935	0.3957	−0.00226		

[a]Reprinted (Adapted or Reprinted in part) with permission from [51]. Copyright [2017] [Elsevier].

https://doi.org/10.1021/acsomega.3c10250
ACS Omega 2024, 9, 16221−16236

$$A = \frac{Q}{UJ\triangle T_M} \tag{26}$$

where A is the heat transfer area, J is the correction coefficient of the heat transfer system, Q is the heat transfer capacity of the equipment, U is the total heat transfer coefficient, and ΔT_M denotes the logarithm of the average temperature difference between the two sides of the fluid in the heat exchanger, The calculation of ΔT_M is as follows:[39]

$$\triangle T_M = \frac{(T_{H,in} - T_{C,out}) - (T_{H,out} - T_{C,in})}{\ln\left(\frac{(T_{H,in} - T_{C,out})}{(T_{H,out} - T_{C,in})}\right)} \tag{27}$$

The heat transfer coefficient for the pure counterflow plate heat exchanger requires no modification[52] The formula for the correction coefficient in the heat transfer system is calculated as follows:[53]

$$J = \frac{\sqrt{(R^2+1)\ln\left(\frac{1-S}{1-RS}\right)}}{(R-1)\ln\left[\frac{2-S(R+1-\sqrt{R^2+1})}{2-S(R+1+\sqrt{R^2+1})}\right]} \tag{28}$$

$$R = \frac{(T_{H,in} - T_{H,out})}{(T_{C,out} - T_{C,in})} \tag{29}$$

$$S = \frac{(T_{C,out} - T_{C,in})}{(T_{H,in} - T_{C,in})} \tag{30}$$

The plate exchanger's total heat transfer coefficient can be calculated as follows:

$$U = \left(\frac{1}{H_{wf}} + \frac{\delta}{\lambda} + \frac{1}{H_s}\right)^{-1} \tag{31}$$

$$H = \mathrm{Nu}\frac{\lambda}{D_e} \tag{32}$$

where H_{wf} is the heat transfer coefficient of the organic work material and H_s is the heat transfer coefficient of the hot gas side or the cold source side. δ is the thickness of the plate. λ is the thermal conductivity of the plate, and D_e is the equivalent diameter of the tube. Nu is the Nussle number.

In the process of heating organic substances by a heat source, the convective heat transfer coefficient on the fluid side is usually more than 2000 W/(m^2·K),[54] which is much larger than the convective heat transfer coefficient on the gas side. Therefore, it is assumed that the total heat transfer coefficient in the evaporation section is the gas-side heat transfer coefficient. On the other hand, the condenser has two important processes: the precooling stage and the cooling stage. In the precooling stage, the heat transfer coefficient on the gaseous organic working fluids side dominates the total heat transfer coefficient, which can be calculated as

$$\mathrm{Nu} = 0.724\left(\frac{6\beta}{\pi}\right)^{0,646}\mathrm{Re}^{0.583}\mathrm{Pr}^{1/3} \tag{33}$$

where β is the herringbone plate corrugation angle and Re and Pr are the Reynolds and Prandtl numbers, respectively.

During the cooling phase, phase change occurs on the organic working fluid side, assuming a phase change coefficient of 5000 W/(m^2·K).[55] However, the heat transfer coefficient of the working fluid where water is the cooling source and no phase change occurs, its heat transfer coefficient, can be calculated as follows:

$$\mathrm{Nu} = 0.42\mathrm{Re}^{0.63}\mathrm{Pr}^{0.3}(200 < \mathrm{Re} < 1200) \tag{34}$$

$$\mathrm{Nu} = 0.42\mathrm{Re}^{0.7}\mathrm{Pr}^{0.3}(1200 < \mathrm{Re} < 20000) \tag{35}$$

Equations 29−33 for the plate heat exchanger are based on the parameters presented in Table 6. Additionally, for the absorption heat pump in the shell and tube heat exchanger, the parameters are detailed in Table 7.

Table 6. Parameters of Plate Heat Exchanger[43a]

parameter	unit	value
thickness of the plate	mm	0.9
channel width	mm	605
distance between flow channels	mm	5
herringbone plate corrugated angle	°	120

[a]Reprinted (Adapted or Reprinted in part) with permission from [43]. Copyright [2021] [Elsevier].

Table 7. Thermodynamic Design Conditions of AHP

parameters	value
temperature difference of evaporator,$\Delta T_{eva,AHE}$ (K)	2.0[59]
temperature difference of condenser,$\Delta T_{con,AHE}$ (K)	5.0[60]
temperature difference of generator,$\Delta T_{eva,AHE}$ (K)	5.0[60]
temperature difference of absorber,$\Delta T_{abs,AHE}$ (K)	5.0[60]
overall heat transfer coefficient of the evaporator, $U_{eva,AHE}$ [W/(m^2·K)]	2791.0[59]
overall heat transfer coefficient of the condenser, $U_{con,AHE}$ [W/(m^2·K)]	5234.0[59]
overall heat transfer coefficient of the absorber, $U_{abs,AHE}$ [W/(m^2·K)]	1163.0[59]
overall heat transfer coefficient of the generator, $U_{gen,AHE}$ [W/(m^2·K)]	1623.0[59]

The cost of the generator:[56]

$$C_{Gen} = 60(W_{Gen})^{0.95} \tag{36}$$

where C_{Gen} and W_{Gen} denote generator cost and generation power, respectively.

To align equipment costs with contemporary market prices, cost adjustments are made by using the Chemical Economics Plant Cost Index (CEPCI). As an illustration, the CEPCI values for 2021[57] and 2000[58] are 699.97 and 394.1, respectively.

$$C_{e,2021} = C_{e,2000}\frac{CEPCI_{2021}}{CEPCI_{2020}} \tag{37}$$

The total cost of a project depends overwhelmingly on the equipment cost of the system. In an ACHP system, the total cost incorporates the cost of the absorption heat exchanger (AHE), the cost of the geothermal well, and the cost of the turbine, condenser, pumps, and other components of the system. The total investment cost is shown in the formula below:

$$C_{tot,ACHP} = C_{GW,RE} + C_{AHE} + C_{tur,ORC} + C_{con,ORC} + C_{pum1} + C_{pum3} \tag{38}$$

https://doi.org/10.1021/acsomega.3c10250
ACS Omega 2024, 9, 16221−16236

$$C_{tot,AHE} = C_{eva,AHE} + C_{abs,AHE} + C_{con,AHE} + C_{gen,AHE} + C_{SHX} + C_{HEX} + C_{pum2} \quad (39)$$

The levelized cost of electricity (LCOE) is used to character the economy of the system, which is expressed as

$$LCOE = \frac{CRF(Z_K + Z_{COM})}{t_{op}W_{net}} \quad (40)$$

where t_{op} is the number of annual operating hours, set to 3650 h. The CRF is calculated by

$$CRF = \frac{i_r(1 + i_r)^{LT}}{(1 + i_r)^{LT} - 1} \quad (41)$$

where i is the annual interest rate of the loan and LT is the life cycle time.

Based on the above conditions, in this paper, a homemade code was written in the MATLAB environment to establish the thermodynamic and economic models of the ACHP system. The thermodynamic properties of the organic work fluid at each state point must be obtained in the calculation process. Therefore, this paper uses the subroutine in REFPROP 9.1 to calculate the thermodynamic parameters of the organic matter. The control variable method is used in the simulation process. For example, when investigating the performance of the system at different heat source temperatures, parameters such as the condensation temperature are kept constant. The fluid properties (e.g., temperature, pressure, enthalpy, exergy, etc.) at each state point of the system can be easily calculated based on the thermodynamic model established above.

3.4. Model Validation. In this study, the results of the ORC and AHP simulations were compared with the experimental results reported by Wang et al.[61] and Lecompte et al.[19] in order to verify the accuracy of the model, as shown in Tables 8 and 9. The results indicate that the maximum relative errors for the ORC system and AHP system are 2.234% and 1.47%, respectively, demonstrating the good accuracy of the model. Parametric analyses were carried out on this basis.

Table 8. Comparison of ORC Models Between the Current Study and those in the Existing Literature

parameter	literature[61]	present model	relative error
heat source temperature (K)	420	420	
evaporator outlet temperature (K)	392.392	392.387	0.001%
evaporation temperature (K)	390.397	390.397	
evaporation pressure (kPa)	1823.419	1823.419	0
condensation pressure (kPa)	177.785	177.785	0
heat source outlet temperature (K)	375.178	374.769	0.109%
flow rate of organic working medium (kg/h)	10116	10342	2.234%

3.5. FAHP-Entropy Model. This study proposes an evaluation model for the FAHP-EWM (fuzzy analytic hierarchy process-entropy weight method) comprehensive assessment approach. The model takes into account both subjective experience and objective facts and considers three decision criteria: (1) LCOE, (2) exergy efficiency, and (3) thermal efficiency, providing a better guidance for the assessment and decision-making in working fluid selection.

Table 9. Comparison of AHP Models Between the Current Study and the Previous Works

parameter	literature[19]	present model	relative error
working fluid temperature at generator (°C)	55.09	55.09	
working fluid temperature at evaporator (°C)	12	12	
working fluid temperature at absorber (°C)	33	33	
working fluid temperature at condenser (°C)	35	35	
absorption efficiency (%)	59	58.13	1.47%

3.5.1. Calculate the Weights Using the Analytic Hierarchy Process. FAHP is a subjective analysis method, and the calculation steps are as follows: Construct the triangular fuzzy function comparison matrix, based on the consideration of multiattribute index comparison, the fuzzy number used is the triangular fuzzy number, two by two comparison of the different criteria by experts.[62] The triangular fuzzy number $M(l, m, u)$ indicates that when $x = m$, x belongs to M completely, l and u are the lower and upper bounds of the triangular fuzzy number, respectively, and when $x \neq (l, u)$, x does not belong to the fuzzy number M. The model uses the triangular fuzzy numbers M_1, M_3, M_5, M_7, M_9 instead of the traditional scaled values of the AHP method, and uses M_2, M_4, M_6, M_8 as AHP method scale intermediate values; the fuzzy comparison matrix is obtained as shown in Table 10.

Table 10. Fuzzy Comparison Matrix[63a]

parameter	implication
M_1	equally priority
M_3	weak priority
M_5	moderate priority
M_7	very strong priority
M_9	absolute priority
M_2, M_4, M_6, M_8	the importance is between the two
reciprocal	if the importance ratio of factor i to factor j is a_{ij}, then the importance ratio of factor j to factor i is $1/a_{ij}$.

[a]Reprinted (Adapted or Reprinted in part) with permission from [63]. Copyright [2022] [Elsevier].

In order to test the reasonableness of the weights, the matrix was subjected to a hierarchical consistency test

$$CI = \frac{\lambda_{max} - n}{n - 1} \quad (42)$$

$$CR = \frac{CI}{RI} \quad (43)$$

where CI (consistency index) is the calculation of consistency index and λ_{max} is the largest eigenvalue of the judgment matrix. According to the eigenvalue to find the corresponding consistency index RI, the consistency ratio CR (consistency ratio) can be obtained. When CR < 0.10, the consistency of the judgment matrix is acceptable; otherwise, the judgment matrix needs to be modified. In the fuzzy evaluation model, the consistency test of the fuzzy judgment matrix can be carried out by replacing the fuzzy numbers with triangular fuzzy numbers centered on real numbers.The fuzzy

https://doi.org/10.1021/acsomega.3c10250
ACS Omega 2024, 9, 16221−16236

matrix (FM) can be obtained according to the results of expert scoring by calculating the following equation:

$$D_i^k = \sum_{j=1}^{n} \frac{a_{ij}^k}{\sum_{i,j=1}^{n} a_{ij}^k} \tag{44}$$

The combined fuzzy value of each indicator is obtained from FM.

Defuzzification, for triangular fuzzy numbers $M1$ and $M2$, there are two-by-two comparisons of fuzzy probability formulas

$$P(M_1 \geq M_2, m_1 \geq m_2) = 0 \tag{45}$$

$$P(M_1 \geq M_2, m_1 \leq m_2, u_1 \geq l_2) = \frac{l_2 - u_1}{(l_2 - u_1) - (l_1 - u_2)} \tag{46}$$

$$P(M_1 \geq M_2, \text{else}) = 0 \tag{47}$$

For triangular fuzzy numbers M_i, when $i \in [1, n]$, there are multinomial comparative fuzzy probability formulas:

$$P(M_1 \geq M_1, M_2, \ldots, M_n) = \min P(M \geq M_i) \tag{48}$$

According to the fuzzy probability, eqs 45−48 can obtain the relative importance degree size of other indicators (weight), after which normalization is carried out to obtain the final weight of each indicator.

3.5.2. Calculate the Weights Using the Entropy Weight method. The entropy method is based on actual data and uses the objective information reflected in each indicator to determine the weights. In information theory, entropy is a measure of the uncertainty. Generally speaking, if the information entropy of an indicator is smaller, it indicates that the more information the indicator value provides, the greater role it can play in the evaluation and the greater its weight. On the contrary, the larger the information entropy of an indicator is, the less information it provides. The specific measurement process is as follows:

In a scenario with m assessment experts and n assessment indicators, where the assessment value of the jth indicator for the ith expert is denoted as X_{ij}, the raw indicator data matrix is defined as follows:

$$\begin{pmatrix} x_{11} & \cdots & x_{1n} \\ \cdots & \cdots & \cdots \\ x_{m1} & \cdots & x_{mn} \end{pmatrix} \tag{49}$$

The types of indicators are generally categorized as very large, very small, intermediate, and intervals. The types of indicators analyzed in this paper are very large and very small indicators; for very large indicators, the larger the value, the better; for very small indicators, the smaller the value, the better; the specific treatment is as follows:

$$\text{Very Large Indicators: } M = X \tag{50}$$

$$\text{Very Small Indicator: } M = \text{Max} - X \tag{51}$$

There are positive and negative indicators when the data are dimensionless. A positive indicator implies that a higher value corresponds to better evaluation results, while a negative indicator indicates the opposite. Equation 50 is employed for positive indicators such as energy efficiency and thermal efficiency, while eq 51 is utilized for negative indicators like ICOE:

$$\tilde{Z}_{ij} = \frac{x_{ij} - \min(x_{1j}, x_{2j}, \ldots, x_{nj})}{\max(x_{1j}, x_{2j}, \ldots, x_{nj}) - \min(x_{1j}, x_{2j}, \ldots, x_{nj})} \tag{52}$$

$$\tilde{Z}_{ij} = \frac{\max(x_{1j}, x_{2j}, \ldots, x_{nj}) - x_{ij}}{\max(x_{1j}, x_{2j}, \ldots, x_{nj}) - \min(x_{1j}, x_{2j}, \ldots, x_{nj})} \tag{53}$$

Data standardization:

$$P_{ij} = \frac{\tilde{Z}_{ij}}{\sum_{i=1}^{n} \tilde{Z}_{ij}} \tag{54}$$

Calculate the information entropy e and information utility d for j indicators

$$e_j = -\frac{1}{\ln n} \sum_{i=1}^{n} p_{ij} \ln(p_{ij}) (j = 1, 2, \ldots, m) \tag{55}$$

$$d_j = 1 - e_j (j = 1, 2, \ldots, m) \tag{56}$$

Calculation of entropy weights:

$$\varphi_j = d_j / \sum_{i=1}^{m} d_j (j = 1, 2, \ldots, m) \tag{57}$$

3.5.3. Calculate the Combined Weight. Combine the weights of fuzzy hierarchical analysis method and entropy weight method to get the combination weight calculation formula is shown in eq 54.

$$W_j = \frac{P_j \varphi_j}{\sum_{j=1}^{n} P_j \varphi_j} \tag{58}$$

4. Results and Discussions. The selection of the working fluid significantly affects the system's performance, and this impact varies depending on the specific working fluid chosen.[64] Hence, choosing the right working fluid entails a balance between environmental considerations, safety factors, physical and chemical characteristics, and the demands of capital investment, manufacturing, and maintenance. Conducting a parametric study is imperative to identifying the suitable working fluid for the ACHP system. According to the "Montreal Protocol" regarding the effect of refrigerants on ozone depletion, these five working fluids have zero ODP (ozone depletion potential represents the relative ability of chlorofluorocarbons in the atmosphere to destroy ozone) and small GWPs (global warming potential is an index of the greenhouse effect of a substance), which make them environmentally friendly work fluid. ODP represents the relative ability of chlorofluorocarbons in the atmosphere to destroy ozone. The most important one is the environmental factors represented by the ODP. According to the current level, it is considered that the refrigerant with an ODP value less than or equal to 0.05 is acceptable. The GWP of the working fluid is generally high, which cannot be avoided. (The GWP of matter is relatively high above 150.) Moreover, Liu et al.[65] demonstrated that if a wet fluid is used in an ORC system, it can damage the turbine during the condensation process. Therefore, only dry fluids are considered in this study. After the above conditions are satisfied, it is of utmost importance that the different working fluids must match the thermodynamic properties of the system due to their different boiling point characteristics. In this study, fluids with unsuitable

https://doi.org/10.1021/acsomega.3c10250
ACS Omega 2024, 9, 16221−16236

Table 11. Properties of Alternative Working Fluids[66a]

substance	physical data: molecular mass (g·mol^{-1})	critical temperature (K)	critical pressure (kPa)	environmental data: GWP	ODP
R1234ze(E)	114.04	382.52	3636.25	<1	0
R152a	66.05	386.41	4516.75	138	0
R22	86.47	369.39	4990	1760	0.034
R245fa	134.05	427.16	3651	858	0
R227ea	170.03	374.9	2925	3500	0

[a]Reprinted (adapted or reprinted in part) with permission from ref66. Copyright (2010) (Elsevier).

physical properties were excluded and five working fluids that can fully participate in the system calculations at all temperature conditions were selected. An analysis of parameters was conducted on five working fluids selected from Table 11, and the results of the system's parameters were discussed. In particular, an analysis was conducted to examine the impact of the geothermal mass flow rate, geothermal source outlet temperature (reinjection geothermal well temperature), heat source outlet temperature from the AHE evaporator, and organic working fluid evaporation temperature parameters on the LCOE, net work, ORC side exergy efficiency, and thermal efficiency of the ACHP system.

4.1. Thermodynamic Analysis. Figures 2−5 illustrate how the net work and electrical efficiency of the system change

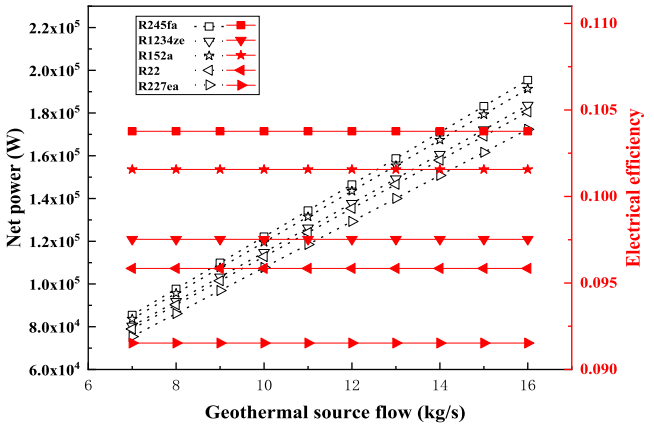

Figure 2. Effects of electrical efficiency and net power with geothermal source flow.

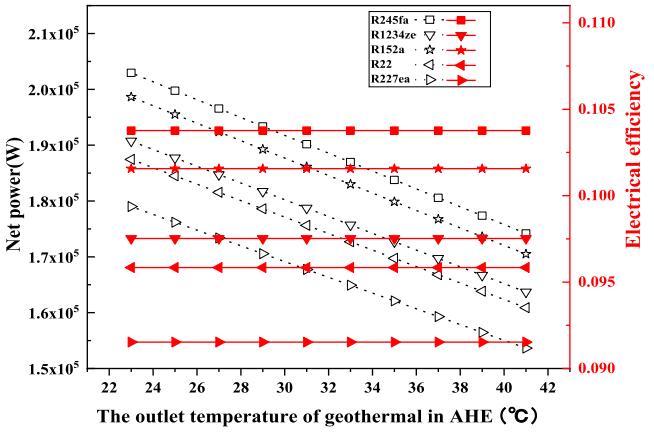

Figure 3. Effects of electrical efficiency and net power with the outlet temperature of geothermal in AHE.

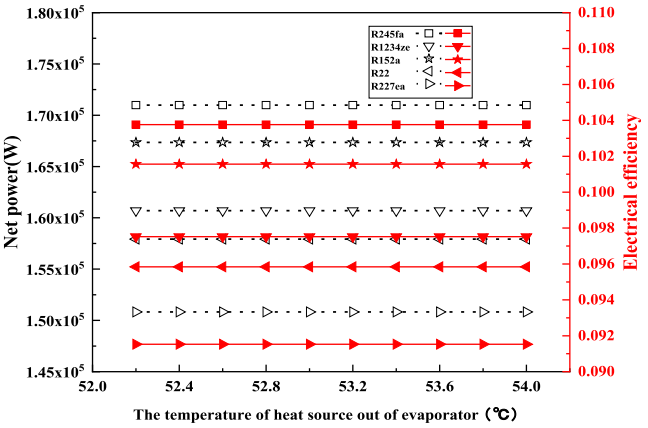

Figure 4. Effects of electrical efficiency and net power with temperature of heat source out of evaporator.

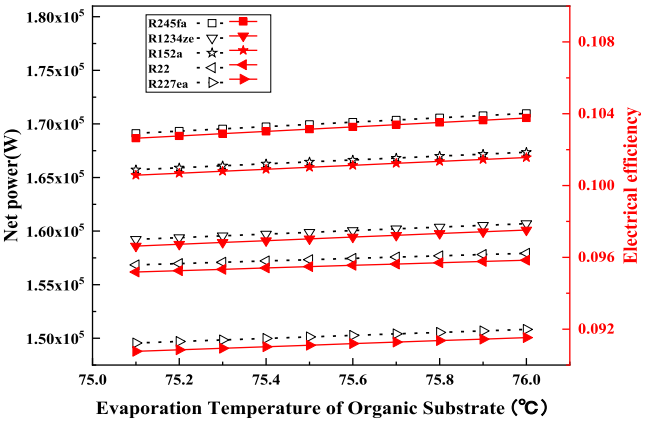

Figure 5. Effects of electrical efficiency and net power with evaporation temperature of organic substrate.

with different parameters for the five work fluids. Figure 2 gives the variation of the net power and electrical efficiency of the system, with respect to the heat source flow rate. It is worth noting that the higher the heat source flow the higher the net power while the electrical efficiency remains constant. Because the flow does not change the working condition and system structure, and the efficiency is calculated by enthalpy, the efficiency does not change. It only affects the size of the heat scale. The larger the flow rate, the higher the heat input at the same temperature, so the work will increase. Figure 3 represents the geothermal out AHE system temperature, which proves that this ACHP system can reduce the heat source outlet temperature to 23 °C. The maximum net work of the system is 202.9 kW when the outlet temperature is 23 °C. The net work of the system decreases with the increase in the temperature of the geothermal wells injected back from the

https://doi.org/10.1021/acsomega.3c10250
ACS Omega 2024, 9, 16221−16236

geothermal source, which is due to the fact that the excess heat from the geothermal heat at high injection temperature is not effectively utilized, and the electrical efficiency does not change when the temperature of the geothermal wells is varied at the reinjected geothermal wells. Figure 4 demonstrates that variation of the heat source at the outlet temperature of the AHE evaporator has no effect on the net work and electrical efficiency of the system. Figure 5 explains the effect of the evaporation temperature of the work fluid on the system. It can be seen that the AHE outlet temperature parameters do not affect the system. When the evaporation temperature of the working fluid changes in this range, the higher the evaporation temperature, the greater the power and efficiency, which is because the working point of the working fluid (T-S diagram performance) changes. And the LiBr/H_2O worker parameter in AHE limits the energy transfer process, resulting in the ORC worker evaporation temperature variation range cannot be too large, which will not be mentioned again in the following analysis. As shown in the figure, the higher the evaporation temperature, the higher the net work and electrical efficiency of the system within the range of the evaporation temperature of the organic work fluid of the system. The parameter of the organic work fluid evaporation temperature increases the electrical efficiency of the system. Among these four parameter ranges, R245fa demonstrates the best performance, with both net work and electrical efficiency surpassing the performance of other working fluids, while R227ea performs the worst.

4.2. Exergy Analysis. Figures 6–9 depict the ACHP system's higher exergy efficiency in ORC power generation. In

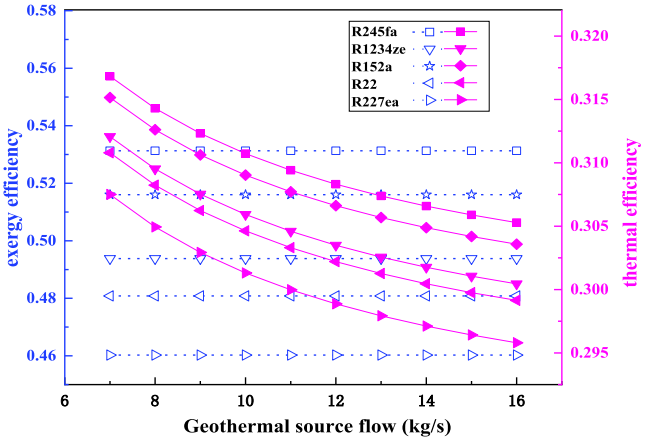

Figure 6. System exergy efficiency and thermal efficiency with geothermal source flow.

Figure 6, it can be seen that the exergy efficiency remains constant with the increase in the flow rate of the ground heat source. The exergy efficiency of the R245fa is the largest, while the R227ea has the smallest exergy efficiency. Whereas, the thermal efficiency of the system decreases as the geothermal heat flow increases, the thermal efficiency decreases from 31.68% to 30.52%. This is due to the decrease in the total ratio of heat source utilized at the heat user end. In Figure 7, the changes in the hydronic efficiency and thermal efficiency show an opposite trend as the temperature of the geothermal out of the AHE system increases. Exergy efficiency decreases with an increase in geothermal outlet temperature of the AHE system, while thermal efficiency increases with the rise in geothermal outlet temperature of the AHE system. When the system uses

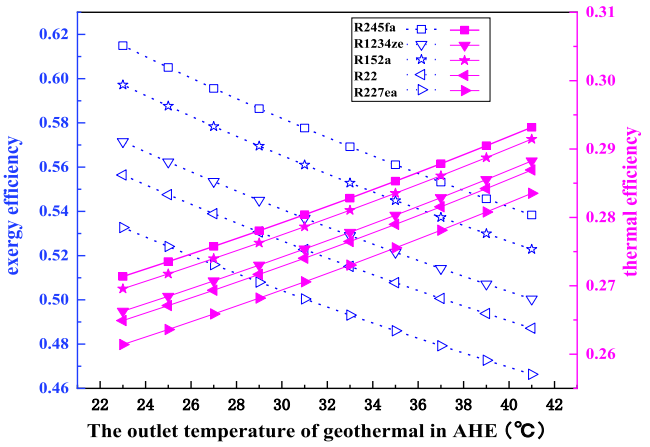

Figure 7. System exergy efficiency and thermal efficiency with outlet temperature of geothermal in AHE.

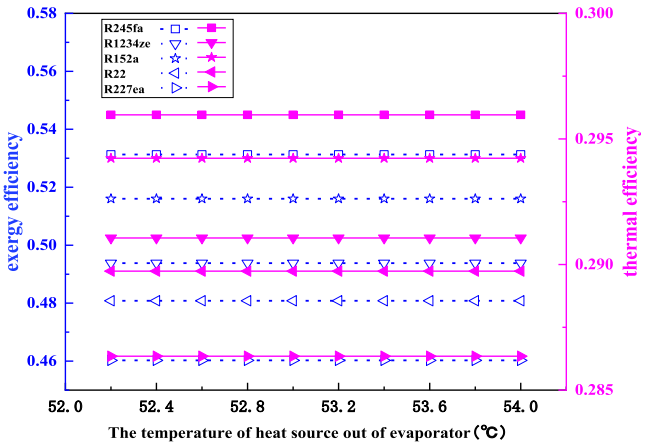

Figure 8. System exergy efficiency and thermal efficiency with temperature of heat source out of evaporator.

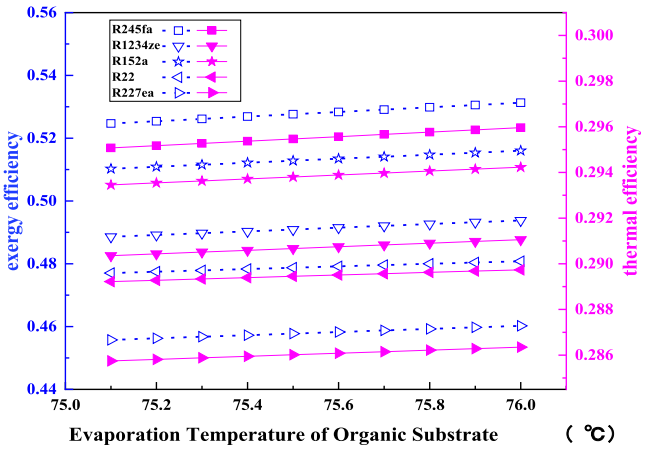

Figure 9. System exergy efficiency and thermal efficiency with evaporation temperature of organic substrate.

R245fa and the outlet temperature of the heat source at 23 °C, the system achieves a maximum exergy-efficiency of 61.39%. Correspondingly, when the temperature of the heat source out of the AHE system is 41 °C, the maximum thermal efficiency of the system is 29.32%. Figure 8 demonstrates that the variation of the heat source's temperature at the evaporator outlet has no effect on the system's exergy efficiency and

https://doi.org/10.1021/acsomega.3c10250
ACS Omega 2024, 9, 16221−16236

thermal efficiency. Whereas, in Figure 9 in the range of evaporation temperature of the organic working fluid, as the evaporation temperature of the working fluid increases, the exergy efficiency and thermal efficiency of the system also increase. The R245fa working fluid still shows excellent performance in the range of these four parameter variations, and the performance of the hydronic efficiency and thermal efficiency is higher than that of the other work fluids.

Figure 10 presents the distribution of the exergy loss in the system. As shown in Figure 10, the maximum percentage of

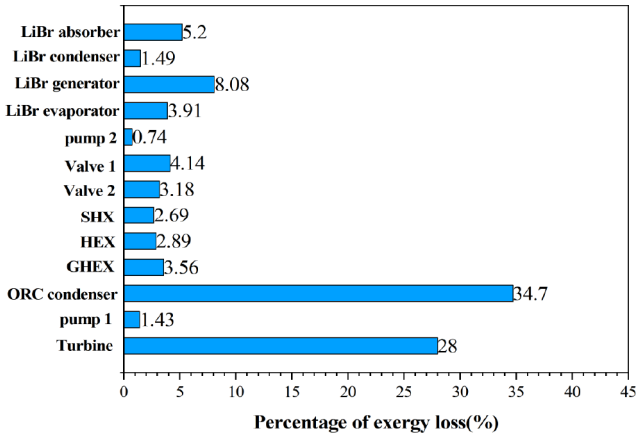

Figure 10. Percentage distribution of the exergy loss.

component loss in the condensing part of the system is 34.7%. In order to reduce this part of the exergy loss, we can adjust the condensation temperature or use the condensation heat of the organic fluid as the ACHP heat source. Furthermore, optimizing the internal flow design of the condenser and altering its configuration can be undertaken to reduce flow resistance and enhance efficiency. In the AHE section, the percentage of generator occupancy exergy loss is up to 8.08%. The generator structure can be further redesigned to adjust the temperature difference for the purpose of mitigating losses in the exergy. The turbine, on the other hand, accounts for 28% of the system's exergy loss. For the exergy losses in the turbine, measures such as implementing advanced lubrication systems and optimizing the design of the turbine stages can be adopted.

4.3. Economic Analysis. Figures 11 and 13 show the LCOE performance of the system for different working fluids at different parameter variations. A lower LCOE indicates better economic system performance. Figure 11 illustrates a significant decrease in the system's EPC as the geothermal heat source flow rate increases, indicating improved economic performance. When the flow increases, the scale of the system becomes larger. Although the system cost increases, the harvested power generation benefits become greater. Therefore, under the condition of constant working conditions, the unit power generation cost will be reduced, so the LCOE will decrease. In Figure 12, it is evident that the R22 work fluid exhibits the best economic performance with a minimum LCOE of 0.082 ($/kW·h). An increase in the geothermal outlet temperature of the AHE system leads to a significant rise in the system's LCOE, resulting in higher costs. This is because when the heat source outlet temperature increases, the thermodynamic performance of the system decreases and energy efficiency will decline, leading to a longer payback period despite the same cost input. This is in line with the

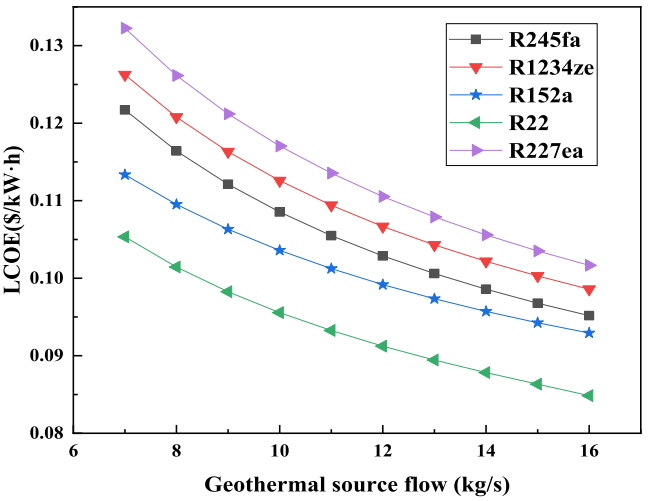

Figure 11. LCOE under different geothermal source flow.

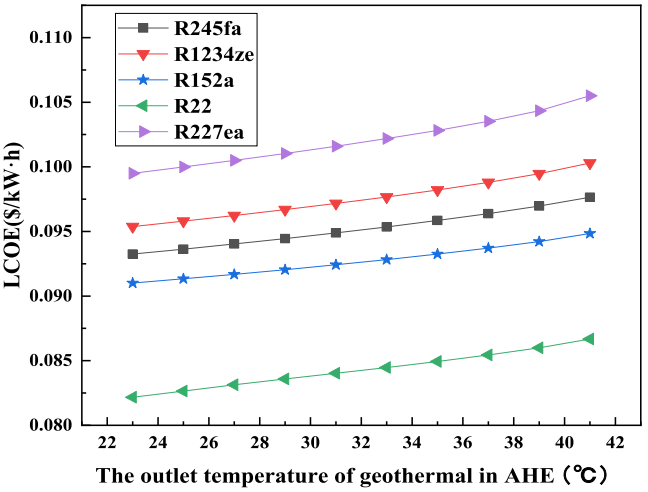

Figure 12. LCOE under outlet temperature of geothermal in AHE.

previous finding that an increase in the AHE outlet temperature results in a decrease in the exergy efficiency of the system's heat source. In Figure 13, when the heat source

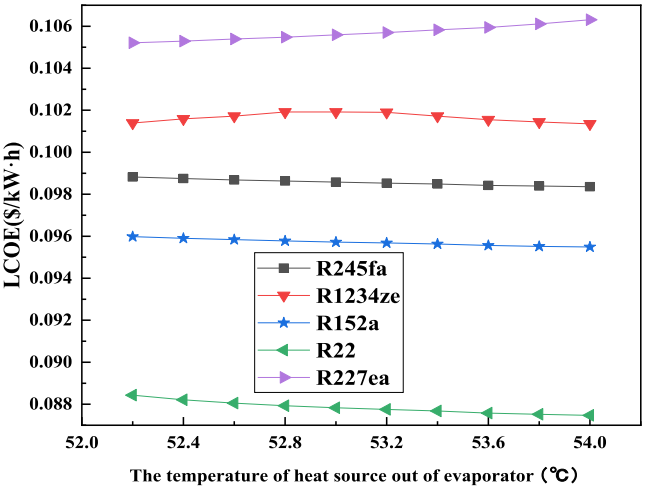

Figure 13. LCOE under outlet temperature of the heat source out of the evaporator.

https://doi.org/10.1021/acsomega.3c10250
ACS Omega 2024, 9, 16221−16236

temperature increases at the evaporator outlet, the change in LCOE varies for different working fluids. This is related to the unique physical property curve of the working fluid, and different physical properties will match the working conditions differently. LCOE continuously increases for R227ea, increases and then decreases for R1234ze, and consistently decreases for the other working fluids. It is worth noting that R245fa, which performs excellently in terms of thermodynamic performance, has an average LCOE performance, while R22 exhibits the best LCOE performance. R227ea, on the other hand, has the poorest LCOE performance.

Under optimal performance conditions with the geothermal heat source operating at 358.15 K, the detailed annual capital cost for each system component is depicted in Figure 14. It can

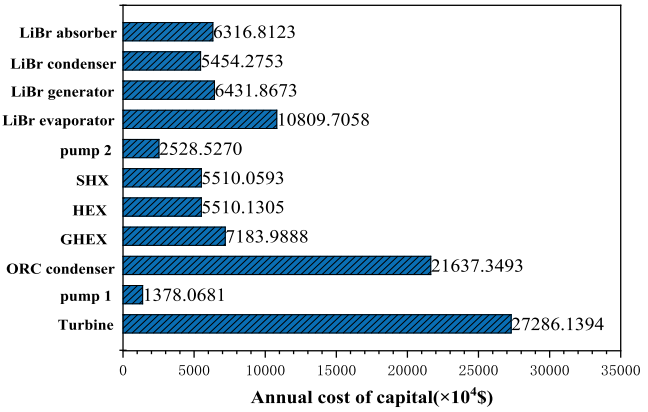

Figure 14. Annual capital cost of each component.

be observed that in the ACHP system, the AHE (ORC condenser) incurs the highest total cost. Meanwhile, in the AHE system, the evaporator and condenser cost constitutes a relatively large proportion. This matches the exergy loss diagram, because the exergy loss of the condensing component is large, resulting in a large economic loss. For future consideration, cost reduction strategies for the AHE evaporator and condenser can be explored.

4.4. Working Fluid Selection Based on the Different Weighting Factors. The main purpose of this section is to discuss the impact of various weight factors in the FAHP-EWM combined weighting method on the selection of working fluids in the system using LCOE, exergy efficiency, and thermal efficiency as evaluation criteria. The parameter results were analyzed and compared under three different weighting factor schemes (LCOE, exergy efficiency, and thermal efficiency). The first scheme balances the weight factors for all three indicators at (0.33, 0.33, and 0.33). The second scheme emphasizes the economic performance of the ACHP system, with weight factors between LCOE, exergy efficiency, and thermal efficiency set at (0.43, 0.26, and 0.31). Similarly, the third scheme primarily focuses on the thermal performance indicator, specifically thermal efficiency, with weight factors arranged as (0.25, 0.33, and 0.42).

As shown in Figure 15 and Table 12, the comprehensive evaluation scores of the five working fluids under the three different weight factor schemes are presented, allowing for a comparison of the overall scores of these five working fluids in the three different weight factor schemes. Whether under balanced weight factors or emphasizing economic or thermodynamic performance, the R245fa working fluid

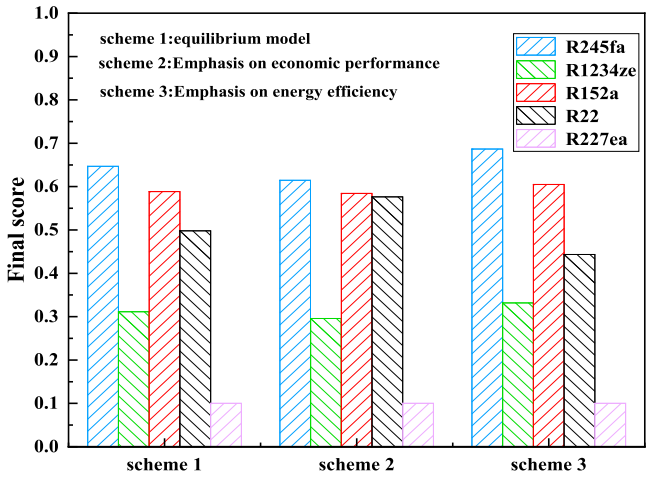

Figure 15. Working fluid evaluation scoring chart.

Table 12. Working Fluid Evaluation Parameter Results

working	final score		
substance	scheme 1 equilibrium model	scheme 2 emphasis on economic performance	scheme 3 emphasis on energy efficiency
R245fa	0.646779074	0.622487621	0.682544916
R1234ze	0.311460093	0.300196143	0.329735164
R152a	0.588392754	0.586933482	0.60359031
R22	0.498079156	0.562646951	0.450559495
R227ea	0.100000001	0.100000001	0.100000001

consistently exhibited the highest and most favorable evaluation scores.

5. CONCLUSIONS

In this paper, an absorption combined heat and power (ACHP) system is proposed in order to make full use of low-temperature geothermal resources. Five working fluids were selected for energy, exergy, and economic analyses of the system. The comprehensive evaluation method FAHP-EWM was applied to evaluate the performance of different working fluids, considering criteria such as LCOE, exergy, efficiency, and thermal efficiency. The goal was to identify the most suitable working fluids for the system. The main conclusions are as follows:

(1) Under given boundary conditions, the FAHP-EWM comprehensive evaluation method is employed to assess the working fluid performance of the ACHP system. The results indicate that, whether emphasizing the economic viability or thermodynamic performance of the working fluid, the optimal working fluid score is consistently R245fa using the comprehensive evaluation method. The ACHP system exhibits high thermal source utilization efficiency, with the geothermal source reaching a minimum temperature of 23 °C at the system outlet. Furthermore, under the operating condition with the minimum outlet temperature of 23 °C using R245fa, the system achieves a maximum net power of 202.9 kW and a peak exergy efficiency of 61.39%. Meanwhile, under the condition of a geothermal flow rate of 7 kg/s, the system attains a maximum thermal efficiency of 31.68%.

https://doi.org/10.1021/acsomega.3c10250
ACS Omega 2024, 9, 16221−16236

(2) In the ACHP system, the primary exergy losses predominantly occur in the condenser and turbine, accounting for 34.7% and 28% of the total exergy loss, respectively. On the other hand, within the AHE system, the highest exergy loss is attributed to the generator, constituting 8.08% of the ACHP system's total exergy loss.

(3) From a sole economic perspective, the R22 working fluid demonstrates optimal economic performance. With an increase in geothermal source flow rate, the economic efficiency of the ORC system improves. When the geothermal source results in a system outlet temperature of 23 °C, the system achieves a minimum LCOE of 0.082 ($/kW·h). When analyzing system costs with the best working fluid, the ORC system exhibits a significant proportion of costs in the condenser and evaporator, while in the AHE system, the major cost components are the evaporator and turbine.

This study provides valuable insights for low-temperature geothermal power generation, demonstrating strong economic viability without relying on local power subsidies. In the future, the choice of working fluid, carbon emissions, system structure, working conditions, materials, and other factors will be further considered. While Azeotropic mixtures will be the focus of the study. Azeotropic mixtures effectively integrate the advantages of individual pure components to realize complementary benefits in terms of environmental sustainability, stability, safety, and thermophysical properties. This assertion has been supported by numerous scholars.[37]

AUTHOR INFORMATION

Corresponding Author

Bing Zhu − *Laboratory for Energy & Power Engineering of Electrical Engineering College, Guizhou University, Guiyang, Guizhou 550025, PR China*; orcid.org/0009-0002-8621-5290; Email: BingZHU_gzu@163.com

Authors

Jiahui Yin − *Laboratory for Energy & Power Engineering of Electrical Engineering College, Guizhou University, Guiyang, Guizhou 550025, PR China*

Yiming Zhang − *Laboratory for Energy & Power Engineering of Electrical Engineering College, Guizhou University, Guiyang, Guizhou 550025, PR China*

Jinsen Huang − *Laboratory for Energy & Power Engineering of Electrical Engineering College, Guizhou University, Guiyang, Guizhou 550025, PR China*

Complete contact information is available at: https://pubs.acs.org/10.1021/acsomega.3c10250

Notes

The authors declare no competing financial interest.

ACKNOWLEDGMENTS

The authors gratefully acknowledge Science and Technology Support Plan Project of Guizhou Province (No. 2017YFB0902100).

NOMENCLATURE

ACHP	absorption combined heat and power
A	circulation ratio
A	heat transfer area, m^2
B	chemical exergy of components, kW
c_p	specific heat capacity at constant pressure, J/(kg·K)
C	cost, $
CI	consistency index
CR	consistency ratio
COP	performance coefficient
E	exergy, kW
F	cost correction parameter
F	cost correction parameter
FM	fuzzy matrix
G	factor of the efficiency correlations
h	enthalpy, kJ/kg
H	heat transfer coefficient correction factor
i	annual interest rate
I	exergy loss, kW
J	heat transfer coefficient correction factor
K	cost correction parameter
L	long
LCOE	levelized discounted electricity generation cost, $/(kW·h)
LT	life cycle time, year
m	mass flow, kg/h
M	cost index
Nu	Nusselt number
p	pressure, kPa
Q	heat, kW
R	heat transfer coefficient correction factor
Re	Reynolds number
S	heat transfer coefficient correction factor
t	time, h
T	temperature, K
U	heat transfer coefficient
W	power, kW
W_j	combined weight
x	mass fraction
z	mole fraction, kJ/mol
Z	cost correction parameter
Z	cost, $

GREEK SYMBOLS

η	efficiency

SUBSCRIPTS

AHE	absorption heat exchanger
abs	absorber
all	all
b	basic
con	condenser
ch	chemical
e	corrected
elc	electric
eva	evaporator
ex	exergy
gen	generator
gw	geothermal water
Gw	geothermal well
H	hot
HEX	heat exchanger
HX-P	plate heat exchangers
HX-S	shell and tube heat exchangers
in	inlet
net	net power

https://doi.org/10.1021/acsomega.3c10250
ACS Omega 2024, 9, 16221−16236

out	outlet
ORC	organic Rankine cycle system
ph	physical
pinch	pinch point
pum	pump
rh	residential heat
Rw	Regenerative well
s	solution
st	steam
sou	heat source
sys	system
SHX	solution heat exchanger
tot	total
tur	turbine
val	valve
wf	working fluid
wh	waste heat

REFERENCES

(1) Lin, S.; Zhao, L.; Deng, S.; Zhao, D.; Wang, W.; Chen, M. Intelligent collaborative attainment of structure configuration and fluid selection for the Organic Rankine cycle. *Appl. Energy* **2020**, *264*, 114743.

(2) Geng, D.; Evans, S. A literature review of energy waste in the manufacturing industry. *Comput. Ind. Eng.* **2022**, *173*, 108713.

(3) Serafino, A.; Obert, B.; Cinnella, P. Multi-fidelity robust design optimization of an ORC turbine for high temperature waste heat recovery. *Energy* **2023**, *269*, 126538.

(4) Michaelides, E. E. Future directions and cycles for electricity production from geothermal resources. *Energy Convers. Manage.* **2016**, *107*, 3−9.

(5) Hou, J.; Cao, M.; Liu, P. Development and utilization of geothermal energy in China: Current practices and future strategies. *Renewable Energy* **2018**, *125*, 401−412.

(6) He, W. F.; Han, D.; Wen, T. Energy, entropy and cost analysis of a combined power and water system with cascade utilization of geothermal energy. *Energy Convers. Manage.* **2018**, *174*, 719−729.

(7) Prananto, L. A.; Juangsa, F. B.; Iqbal, R. M.; Aziz, M.; Soelaiman, T. A. F. Dry steam cycle application for excess steam utilization: Kamojang geothermal power plant case study. *Renewable Energy* **2018**, *117*, 157−165.

(8) Bertani, R. Geothermal power generation in the world 2010−2014 update report. *Geothermics* **2016**, *60*, 31−43.

(9) Ren, C.; Wang, J.; Chen, H.; Liu, X.; An, M. Thermodynamic analysis and comparative investigation of a new combined heating and power system driving by medium -and -high temperature geothermal water. *Energy Convers. Manage.* **2021**, *233*, 113914.

(10) Pan, S.-Y.; Gao, M.; Shah, K. J.; Zheng, J.; Pei, S.-L.; Chiang, P.-C. Establishment of enhanced geothermal energy utilization plans: Barriers and strategies. *Renewable Energy* **2019**, *132*, 19−32.

(11) Fiaschi, D.; Lifshitz, A.; Manfrida, G.; Tempesti, D. An innovative ORC power plant layout for heat and power generation from medium- to low-temperature geothermal resources. *Energy Convers. Manage.* **2014**, *88*, 883−893.

(12) Angrisani, G.; Diglio, G.; Sasso, M.; Calise, F.; d'Accadia, M. D. Design of a novel geothermal heating and cooling system: Energy and economic analysis. *Energy Convers. Manage.* **2016**, *108*, 144−159.

(13) Habka, M.; Ajib, S. Determination and evaluation of the operation characteristics for two configurations of combined heat and power systems depending on the heating plant parameters in low-temperature geothermal applications. *Energy Convers. Manage.* **2013**, *76*, 996−1008.

(14) Eyerer, S.; Schifflechner, C.; Hofbauer, S.; Bauer, W.; Wieland, C.; Spliethoff, H. Combined heat and power from hydrothermal geothermal resources in Germany: An assessment of the potential. *Renewable Sustainable Energy Rev.* **2020**, *120*, 109661.

(15) Wang, J.; Dai, Y.; Gao, L. Exergy analyses and parametric optimizations for different cogeneration power plants in cement industry. *Appl. Energy* **2009**, *86*, 941−948.

(16) Zhang, M.-G.; Zhao, L.-J.; Xiong, Z. Performance evaluation of organic Rankine cycle systems utilizing low grade energy at different temperature. *Energy* **2017**, *127*, 397−407.

(17) Hu, K.; Zhu, J.; Zhang, W.; Liu, K.; Lu, X. Effects of evaporator superheat on system operation stability of an organic Rankine cycle. *Appl. Therm. Eng.* **2017**, *111*, 793−801.

(18) Zhang, X.; Wang, L.; Wang, Z.; Wang, L.; Zhang, Z. Non-steady thermodynamic characteristics of a pilot-scale organic Rankine cycle system with a thermally-driven pump. *Energy* **2022**, *252*, 123993.

(19) Lecompte, S.; Huisseune, H.; van den Broek, M.; Vanslambrouck, B.; De Paepe, M. Review of organic Rankine cycle (ORC) architectures for waste heat recovery. *Renewable Sustainable Energy Rev.* **2015**, *47*, 448−461.

(20) Desai, N. B.; Bandyopadhyay, S. Process integration of organic Rankine cycle. *Energy* **2009**, *34*, 1674−1686.

(21) Javanshir, A.; Sarunac, N.; Razzaghpanah, Z. Thermodynamic analysis of a regenerative organic Rankine cycle using dry fluids. *Appl. Therm. Eng.* **2017**, *123*, 852−864.

(22) Hu, B.; Guo, J.; Yang, Y.; Shao, Y. Selection of working fluid for organic Rankine cycle used in low temperature geothermal power plant. *Energy Rep.* **2022**, *8*, 179−186.

(23) Zhao, Y.; Gao, C.; Li, C.; Sun, J.; Wang, C.; Liu, Q.; Zhao, J. Energy and Exergy Analyses of Geothermal Organic Rankine Cycles Considering the Effect of Brine Reinjection Temperature. *Energies* **2022**, *15* (17), 6230.

(24) Guzović, Z.; Rasković, P.; Blatarić, Z. The comparision of a basic and a dual-pressure ORC (Organic Rankine Cycle): Geothermal Power Plant Velika Ciglena case study. *Energy* **2014**, *76*, 175−186.

(25) Eyerer, S.; Dawo, F.; Wieland, C.; Spliethoff, H. Advanced ORC architecture for geothermal combined heat and power generation. *Energy* **2020**, *205*, 117967.

(26) Van Erdeweghe, S.; Van Bael, J.; Laenen, B.; D'haeseleer, W. Optimal combined heat-and-power plant for a low-temperature geothermal source. *Energy* **2018**, *150*, 396−409.

(27) Ma, R. Q.; Hua, Y.; Yu, X. H.; Zhang, H. T. Performance assessment and multi-objective optimization of a geothermal-based tri-generation system in hot Summer Continental Climate: Tianjin case study. *Energy Convers. Manage.* **2022**, *269*, 116083.

(28) Navarro-Esbrí, J. *4th International Seminar on ORC Power Systems (ORC)*; Exergy, 2017; 652659.

(29) Van Erdeweghe, S.; Van Bael, J.; Laenen, B.; D'haeseleer, W. Comparison of series/parallel configuration for a low-T geothermal CHP plant, coupled to thermal networks. *Renewable Energy* **2017**, *111*, 494−505.

(30) Sun, J.; Fu, L.; Zhang, S. G. Experimental study of heat exchanger basing on absorption cycle for CHP system. *Appl. Therm. Eng.* **2016**, *102*, 1280−1286.

(31) Xie, X.; Jiang, Y. Absorption heat exchangers for long-distance heat transportation. *Energy* **2017**, *141*, 2242−2250.

(32) Zhang, H.; Liu, X.; Liu, Y.; Duan, C.; Dou, Z.; Qin, J. Energy and exergy analyses of a novel cogeneration system coupled with absorption heat pump and organic Rankine cycle based on a direct air cooling coal-fired power plant. *Energy* **2021**, *229*, 120641.

(33) Dogbe, E. S.; Mandegari, M.; Görgens, J. F. Assessment of the thermodynamic performance improvement of a typical sugar mill through the integration of waste-heat recovery technologies. *Appl. Therm. Eng.* **2019**, *158*, 113768.

(34) Khalilzadeh, S.; Nezhad, A. H.; Romagnoli, A.; Akhmetov, B. Investigating the effects of integrating an absorption heat transformer with a combined cooling, heating and power system: A thermodynamic and economic analysis. *Energy Convers. Manage.* **2021**, *228*, 113677.

(35) Tian, W.; Teng, S.; Xi, H. Cogeneration system based on large temperature difference heat transfer with stepwise utilization. *Energy Convers. Manage* **2023**, *281*, 116843.

https://doi.org/10.1021/acsomega.3c10250
ACS Omega 2024, 9, 16221−16236

(36) Wang, S.; Liu, C.; Tang, J.; Xiao, T.; Huo, E.; Guan, Z. Multi-mode and exergoeconomic analysis of a novel combined cooling, heating, and power system applied in the geothermal field. *Energy Convers. Manage.* **2023**, *276*, 116565.
(37) Wang, S.; Tang, J.; Liu, C.; Li, Q.; Sun, Z.; Huo, E. Techno-economic-environmental analysis and fluid selection of transcritical organic Rankine cycle with zeotropic mixtures. *J. Cleaner Prod.* **2024**, *436*, 140690.
(38) Wiley Library *American society of heating, refrigerating and air-conditioning engineers*; Wiley, 1979; Vol. 2, pp. 5657.
(39) Li, J.; Liu, Q.; Duan, Y.; Yang, Z. Performance analysis of organic Rankine cycles using R600/R601 a mixtures with liquid-separated condensation. *Appl. Energy* **2017**, *190*, 376−389.
(40) Xi, H.; Li, M.-J.; Xu, C.; He, Y.-L. Parametric optimization of regenerative organic Rankine cycle (ORC) for low grade waste heat recovery using genetic algorithm. *Energy* **2013**, *58*, 473−482.
(41) Tang, J.; Zhang, Q.; Zhang, Z.; Li, Q.; Wu, C.; Wang, X. Development and performance assessment of a novel combined power system integrating a supercritical carbon dioxide Brayton cycle with an absorption heat transformer. *Energy Convers. Manage.* **2022**, *251*, 114992.
(42) Chitgar, N.; Hemmati, A.; Sadrzadeh, M. A comparative performance analysis, working fluid selection, and machine learning optimization of ORC systems driven by geothermal energy. *Energy Convers. Manage.* **2023**, *286*, 117072.
(43) Teng, S.; Wang, M.; Xi, H.; Wen, S. Energy, exergy, economic (3E) analysis, optimization and comparison of different ORC based CHP systems for waste heat recovery. *Case Stud. Therm. Eng.* **2021**, *28*, 101444.
(44) Zhu, Y.; Li, W.; Li, J.; Li, H.; Wang, Y.; Li, S. Thermodynamic analysis and economic assessment of biomass-fired organic Rankine cycle combined heat and power system integrated with CO_2 capture. *Energy Convers. Manage.* **2020**, *204*, 112310.
(45) Guo, P.; Sui, J.; Han, W.; Zheng, J.; Jin, H. Energy and exergy analyses on the off-design performance of an absorption heat transformer. *Appl. Therm. Eng.* **2012**, *48*, 506−514.
(46) Yu, M.; Chen, Z.; Yao, D.; Zhao, F.; Pan, X.; Liu, X.; Cui, P.; Zhu, Z.; Wang, Y. Energy, exergy, economy analysis and multi-objective optimization of a novel cascade absorption heat transformer driven by low-level waste heat. *Energy Convers. Manage.* **2020**, *221*, 113162.
(47) Jimenez, I. M.; Greenman, J.; Ieropoulos, I. Electricity and catholyte production from ceramic MFCs treating urine. *Int. J. Hydrogen Energy* **2017**, *42* (3), 1791−1799.
(48) Díaz, V. M. A.et al.in ASME International Mechanical Engineering Congress and Exposition (IMECE2015)2016
(49) National public service platform for standards information 2023. https://std.samr.gov.cn/gb/search/gbDetailed?id=71F772D81A39D3A7E05397BE0A0AB82A.
(50) Beijing Municipal People's Government Portal 2023. https://www.beijing.gov.cn/so/s?tab=all&siteCode=1100000088&qt=%E4%BE%9B%E7%83%AD.
(51) Zhang, C.; Liu, C.; Wang, S. K.; Xu, X. X.; Li, Q. B. Thermo-economic comparison of subcritical organic Rankine cycle based on different heat exchanger configurations. *Energy* **2017**, *123*, 728−741.
(52) Nazari, N.; Mousavi, S.; Mirjalili, S. Exergo-economic analysis and multi-objective multi-verse optimization of a solar/biomass-based trigeneration system using externally-fired gas turbine, organic Rankine cycle and absorption refrigeration cycle. *Appl. Therm. Eng.* **2021**, *191*, 116889.
(53) Fettaka, S.; Thibault, J.; Gupta, Y. Design of shell-and-tube heat exchangers using multiobjective optimization. *Int. J. Heat Mass Transfer* **2013**, *60*, 343−354.
(54) Xi, H.; Li, M.-J.; He, Y.-L.; Zhang, Y.-W. Economical evaluation and optimization of organic Rankine cycle with mixture working fluids using R245fa as flame retardant. *Appl. Therm. Eng.* **2017**, *113*, 1056−1070.
(55) Little, A. B.; Garimella, S. Comparative assessment of alternative cycles for waste heat recovery and upgrade. *Energy* **2011**, *36* (7), 4492−4504.
(56) Le, V. L.; Kheiri, A.; Feidt, M.; Pelloux-Prayer, S. Thermodynamic and economic optimizations of a waste heat to power plant driven by a subcritical ORC (Organic Rankine Cycle) using pure or zeotropic working fluid. *Energy* **2014**, *78*, 622−638.
(57) Junsittiwate, R.; Srinophakun, T. R.; Sukpancharoen, S. Techno-economic, environmental, and heat integration of palm empty fruit bunch upgrading for power generation. *Energy Sustainable Dev.* **2022**, *66*, 140−150.
(58) Hou, S.; Cao, S.; Yu, L.; Zhou, Y.; Wu, Y.; Zhang, F. Performance optimization of combined supercritical CO_2 recompression cycle and regenerative organic Rankine cycle using zeotropic mixture fluid. *Energy Convers. Manage.* **2018**, *166*, 187−200.
(59) Wu, Z.; Wang, Y.; You, S.; Zhang, H.; Zheng, X.; Guo, J.; Wei, S. Thermo-economic analysis of composite district heating substation with absorption heat pump. *Appl. Therm. Eng.* **2020**, *166*, 114659.
(60) Chaiyat, N.; Inthavideth, X. The 1st Conference on Heat Energy and Mass Transfer in Thermal Equipment and ProcessesVol. *15*
(61) Wang, S.; Xie, X.; Jiang, Y. Optimization design of the large temperature lift/drop multi-stage vertical absorption temperature transformer based on entransy dissipation method. *Energy* **2014**, *68*, 712−721.
(62) Marenco-Porto, C. A.; Nieto-Londoño, C.; Lopera, L.; Escudero-Atehortua, A.; Giraldo, M.; Jouhara, H. Evaluation of Organic Rankine Cycle alternatives for the cement industry using Analytic Hierarchy Process (AHP) methodology and energy-economic-environmental (3E) analysis. *Energy* **2023**, *281*, 128304.
(63) Wang, S.; Liu, C.; Zhang, S.; Li, Q.; Huo, E. Multi-objective optimization and fluid selection of organic Rankine cycle (ORC) system based on economic-environmental-sustainable analysis. *Energy Convers. Manage.* **2022**, *254*, 115238.
(64) Mazur, V. A.; Nikitin, D. Sustainable Working Media Selection for Renewable Energy Technologies. 2011.
(65) Liu, B.-T.; Chien, K.-H.; Wang, C.-C. Effect of working fluids on organic Rankine cycle for waste heat recovery. *Energy* **2004**, *29*, 1207−1217.
(66) Chen, H.; Goswami, D. Y.; Stefanakos, E. K. A review of thermodynamic cycles and working fluids for the conversion of low-grade heat. *Renewable Sustainable Energy Rev.* **2010**, *14*, 3059−3067.

https://doi.org/10.1021/acsomega.3c10250
ACS Omega 2024, 9, 16221−16236